

OPEN ACCESS

Faster Lead-Acid Battery Simulations from Porous-Electrode Theory: Part I. Physical Model

To cite this article: Valentin Sulzer *et al* 2019 *J. Electrochem. Soc.* **166** A2363

View the [article online](#) for updates and enhancements.



Faster Lead-Acid Battery Simulations from Porous-Electrode Theory: Part I. Physical Model

Valentin Sulzer,^{1,*} S. Jon Chapman,^{1,2} Colin P. Please,^{1,2} David A. Howey,^{2,3,**} and Charles W. Monroe^{2,3,**}

¹Mathematical Institute, University of Oxford, Oxfordshire OX2 6GG, United Kingdom

²The Faraday Institution Didcot, OX11 0RA, United Kingdom

³Department of Engineering Science, University of Oxford, Oxfordshire OX1 3PJ, United Kingdom

An isothermal porous-electrode model of a discharging lead-acid battery is presented, which includes an extension of concentrated-solution theory that accounts for excluded-volume effects, local pressure variation, and a detailed microscopic water balance. The approach accounts for three typically neglected physical phenomena: convection, pressure diffusion, and variation of liquid volume with state of charge. Rescaling of the governing equations uncovers a set of fundamental dimensionless parameters that control the battery's response. For the discharge situations considered here, total volume change and nonuniform pressure effects prove to be negligible because variations occur in just one spatial dimension. A numerical solution of a simplified model is developed and exploited to predict transient cell voltages and internal concentration profiles in response to a range of C-rates. The dependence of discharge capacity on C-rate deviates substantially from Peukert's simple power law: charge capacity is concentration-limited at low C-rates, and voltage-limited at high C-rates. The model is fit to experimental data, showing good agreement.

© The Author(s) 2019. Published by ECS. This is an open access article distributed under the terms of the Creative Commons Attribution 4.0 License (CC BY, <http://creativecommons.org/licenses/by/4.0/>), which permits unrestricted reuse of the work in any medium, provided the original work is properly cited. [DOI: 10.1149/2.0301910jes]



Manuscript submitted February 5, 2019; revised manuscript received May 12, 2019. Published July 3, 2019.

Lead-acid batteries are the most widely used electrochemical storage technology, with applications including car batteries and off-grid energy supply. Models can improve battery management—for example, by minimizing overcharge to extend cycle life.

The most rigorous mechanistic approach to battery-cell modeling begins with a detailed microscopic description, wherein the electrolyte and electrodes occupy discrete spatial domains; volume averaging is then performed to produce a macroscopic model.^{1–3} The details are beyond the present scope, but such a homogenization underpins the model presented below.

Our development of a detailed macrohomogeneous model of a typical lead-acid battery augments standard approaches by explicitly considering the balance of water, the variation of acid density with molarity, and the distribution of pressure. As well as ensuring thermodynamic consistency and retaining model closure when systems span multiple spatial dimensions,⁴ this reveals novel convective phenomena that may occur at high discharge currents.

Nondimensionalization of the model helps to assess the relative importances of different multiphysical phenomena within it. This facilitates numerical implementation because it greatly improves the conditioning of the system, and hence improves the speed of computations, by making most dependent variables close to unity. This paper focuses on the development of a detailed nonisobaric physical model of battery discharge. A novel nondimensionalization is presented, which helps to identify the key dimensionless parameters that control the battery's transient response. Finally, a numerical procedure is developed to solve the nonlinear system of partial differential equations comprising the model. The results are fit against experimental discharge data and used to show how discharge capacity depends on C-rate. The nonlinear model shows that the battery response does not satisfy Peukert's law. Instead, the capacity follows one power law at low C-rates, where average acid concentration controls the response, and a different power law at high C-rates, where overpotentials control the response.

Below it is shown that coupled pressure effects can be neglected, on the basis that certain dimensionless parameters are small for the materials used in the battery considered here. However, excluded-volume effects remain in the model; the local variation of water concentration in the electrolyte contributes significantly to interfacial reaction kinetics and also impacts diffusion overpotentials. In cases where dimen-

sionless parameters in a model are small or large, asymptotic analysis can be employed, producing simplified, more computationally efficient models that achieve the same level of physical accuracy. The nonlinear model presented here serves as the baseline for testing a hierarchy of computationally efficient reduced-order models, which will be developed by perturbation expansion in part II.⁵

Model

Unscaled governing system.—Battery configuration and chemistry.—

Typically, a valve regulated lead-acid battery comprises six 2 V cells wired in series. Figure 1 depicts one such cell, which consists of five lead (Pb) electrodes and four lead dioxide (PbO₂) electrodes, sandwiched alternately around a porous, electrically insulating separator to produce eight electrode pairs, wired in parallel at the top edge of the electrode pile. The pile has height H , depth W , and cross-sectional area $A_{cs} = HW$. The negative (Pb) and positive (PbO₂) electrodes have half-widths l_n and l_p respectively, and the separator has width l_{sep} , giving each internal electrode pair total width $L = l_n + l_{sep} + l_p$. The layers repeat periodically, allowing the whole pile to be modeled via analysis of one electrode pair. Some thermal effects have been documented experimentally^{6,7} and considered theoretically;^{8,9} we assume an isothermal system for simplicity.

The electrodes are porous, permeated by an aqueous sulfuric acid (H₂SO₄) electrolyte that also permeates the separator. The negative

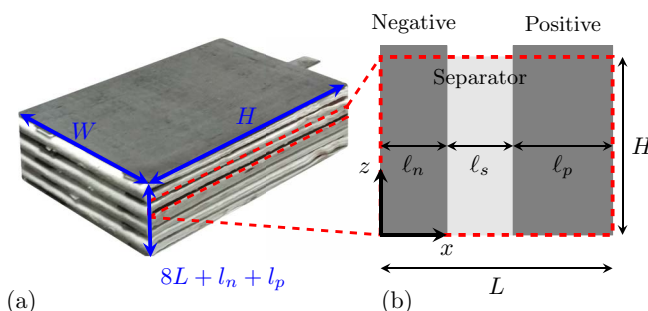


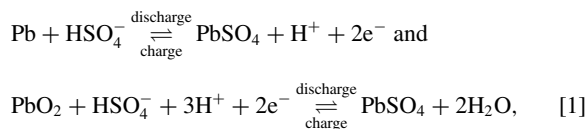
Figure 1. Geometry of a lead-acid cell. (a) A whole lead-acid cell (Photograph by Ashley Grealish, BBOXX). The total width of the cell is $8L + l_n + l_p$ because l_n and l_p are electrode half-widths. (b) A single electrode pair. The y-axis is into the page.

*Electrochemical Society Student Member.

**Electrochemical Society Member.

^zE-mail: sulzer@maths.ox.ac.uk

and positive half-reactions are



respectively. In both reactions, solid lead sulfate (PbSO_4) forms during discharge as bisulfate anions (HSO_4^-) leave the liquid.

Without competitive chemistry, Reaction 1 would simply reverse during recharge, as indicated. However, some authors^{8,10–12} have observed that gas evolution can become important when recharging. To avoid the need for considering such side reactions, the present analysis is limited to discharges.

Liquid thermodynamics.—In water (H_2O), H_2SO_4 dissociates mainly to hydrogen cations (H^+) and HSO_4^- ; in keeping with prior models,^{10,13–15} speciation to sulfate is neglected. Thus the pore-filling liquid comprises H_2O , HSO_4^- , and H^+ , with partial molar volumes \bar{V}_w , \bar{V}_- and \bar{V}_+ , molar masses M_w , M_- , and M_+ , and equivalent charges 0, -1 , and $+1$, respectively. Unscaled variables are denoted with a hat: for example, the species molarities are \hat{c}_w , \hat{c}_- , and \hat{c}_+ .

On a scale much larger than the Debye length, local electroneutrality holds in the liquid phase. Both ion concentrations then relate to the H_2SO_4 molarity \hat{c} through

$$\hat{c} = \hat{c}_+ = \hat{c}_-. \quad [2]$$

In an isothermal state, thermodynamic consistency of the liquid volume requires that \hat{c}_w depends on \hat{c} alone if the bulk modulus of the liquid is very large,¹⁶ through

$$\hat{c}_w = \frac{1 - \bar{V}_e \hat{c}}{\bar{V}_w}, \quad [3]$$

where $\bar{V}_e = \bar{V}_+ + \bar{V}_-$ is the partial molar volume of the acid. Consequently the total liquid molarity $\hat{c}_T = 2\hat{c} + \hat{c}_w$ also depends only on \hat{c} . Acid molarity further determines the mass density $\hat{\rho}$ of the liquid, because

$$\hat{\rho} = \hat{c}_w M_w + \hat{c} M_e = \frac{M_w}{\bar{V}_w} + \left(\frac{M_e}{\bar{V}_e} - \frac{M_w}{\bar{V}_w} \right) \bar{V}_e \hat{c}, \quad [4]$$

in which $M_e = M_+ + M_-$ stands for the acid's molar mass. Experiments show that $\hat{\rho}$ varies almost linearly with \hat{c} ,¹⁷ so the partial molar volumes can be assumed constant.

The mechanical state of the liquid is described by the external pressure \hat{p} , while its mixing free energy is parameterized by a thermodynamic Darken factor $\hat{\chi}(\hat{c})$.

Balances.—The position \hat{x} within each electrode pair traverses three subdomains: the negative electrode ($0 < \hat{x} < l_n$), separator ($l_n < \hat{x} < L - l_p$), and positive electrode ($L - l_p < \hat{x} < L$). The model structure is identical in each subdomain. Parameters describing the electrolyte are similar everywhere, while those describing pore geometry generally differ among subdomains; quantities that parameterise reactions differ between the negative- and positive-electrode subdomains, and vanish in the separator.

Liquid volume fraction $\hat{\varepsilon}$ and reactive solid area per volume \mathcal{A} characterize the homogenized geometry within the electrode pair. In electrode subdomains, deposition (removal) of solid PbSO_4 on pore surfaces is accompanied by removal (deposition) of solid Pb or PbO_2 , so these geometric parameters can generally vary locally. Solid PbSO_4 does not tend to deposit as a compact thin film, so mechanistic lead-acid battery models usually let \mathcal{A} vary with state of charge.^{10,12–15} Since the functionality of this variation is disputed, we instead let the area be constant, following the approach of Liu et al., who showed that the assumption suffices to model Li/O_2 -battery discharge.¹⁸ From this perspective \mathcal{A} describes an immobile Gibbs dividing surface that partitions the layers of Pb or PbO_2 , which contribute to the battery's charge state, from the current-collecting Pb layer beneath them, which does not. Thus the time change in pore volume relates to the molar

volumes of the solid species in Scheme 1 through

$$\frac{1}{\mathcal{A}} \frac{\partial \hat{\varepsilon}}{\partial t} = -\bar{V}_{\text{PbSO}_4} \hat{S}_{\text{PbSO}_4} - \bar{V}_{\text{Pb}} \hat{S}_{\text{Pb}} - \bar{V}_{\text{PbO}_2} \hat{S}_{\text{PbO}_2}, \quad [5]$$

in which \bar{V}_k is the partial molar volume of species k and \hat{S}_k is the rate at which k is generated by interfacial reactions per unit of pore area.

After homogenization, the local mass balance of species $k \in \{w, -, +\}$ in the pore-filling liquid phase implies that

$$\frac{\partial}{\partial t}(\hat{\varepsilon} \hat{c}_k) = -\hat{\nabla} \cdot \hat{\mathbf{N}}_k + \mathcal{A} \hat{S}_k, \quad [6]$$

where $\hat{\mathbf{N}}_k$ represents the molar flux of k . With electroneutrality condition 2 and equation of state 3, all three balance Equations 6 combine to show liquid-volume continuity,

$$\frac{\partial \hat{\varepsilon}}{\partial t} = -\hat{\nabla} \cdot \hat{\mathbf{v}}^\square + \mathcal{A}(\bar{V}_w \hat{S}_w + \bar{V}_- \hat{S}_- + \bar{V}_+ \hat{S}_+), \quad [7]$$

in which $\hat{\mathbf{v}}^\square = \bar{V}_w \hat{\mathbf{N}}_w + \bar{V}_- \hat{\mathbf{N}}_- + \bar{V}_+ \hat{\mathbf{N}}_+$ signifies the volume-averaged liquid velocity.

Under Faraday's law, ion balances 6 also combine to demonstrate charge continuity in the liquid,

$$\hat{\nabla} \cdot \hat{\mathbf{i}} = \mathcal{A} \hat{j}. \quad [8]$$

Letting F be Faraday's constant, the liquid-phase current density is $\hat{\mathbf{i}} = F(\hat{\mathbf{N}}_+ - \hat{\mathbf{N}}_-)$ and the current density associated with interfacial charge exchange is $\hat{j} = F(\hat{S}_+ - \hat{S}_-)$. (Positive \hat{j} flows into pores.) Note that any current leaving the liquid at a given location enters the solid there. Thus

$$\hat{\nabla} \cdot \hat{\mathbf{i}}_s = -\mathcal{A} \hat{j}, \quad [9]$$

where $\hat{\mathbf{i}}_s$ is the solid-phase current density.

In a general isothermal setting, liquid convection is determined by a momentum balance, such as Cauchy's equation.^{4,16} Such a balance governs the distribution of momentum density $\hat{\rho} \hat{\mathbf{v}}$, which is naturally expressed in terms of the mass-averaged velocity $\hat{\mathbf{v}}$. The kinematic relation

$$\begin{aligned} \hat{\mathbf{v}} - \hat{\mathbf{v}}^\square &= \frac{\bar{V}_e}{\hat{\rho}} \left(\frac{M_e}{\bar{V}_e} - \frac{M_w}{\bar{V}_w} \right) (\hat{\mathbf{N}}_+ - \hat{\mathbf{v}}^\square) \\ &\quad + \frac{\bar{V}_-}{\hat{\rho}} \left(\frac{M_w}{\bar{V}_w} - \frac{M_-}{\bar{V}_-} \right) \frac{\hat{\mathbf{i}}}{F} \end{aligned} \quad [10]$$

specifies how $\hat{\mathbf{v}}$ must relate to $\hat{\mathbf{v}}^\square$.

Flux constitutive laws.—Two Onsager–Stefan–Maxwell flux laws govern transport in the liquid phase. The law for the thermodynamic force on water¹⁶ can be inverted¹⁹ to give

$$\hat{\mathbf{N}}_+ = -\hat{D}^{\text{eff}} \left(\hat{\nabla} \hat{c} - \frac{\hat{\psi} \hat{\nabla} \hat{p}}{RT \hat{\chi}} \right) + \frac{t_+^w \hat{\mathbf{i}}}{F} + \hat{c} \hat{\mathbf{v}}^\square, \quad [11]$$

where R is the gas constant, T is the absolute temperature, t_+^w is the cation transference number relative to the water velocity, and \hat{D}^{eff} is the effective Fickian diffusivity of acid in water; the pressure-diffusion factor $\hat{\psi}$ depends on \hat{c} through

$$\hat{\psi} = \frac{\bar{V}_w \hat{c}_T M_w \hat{c}_w M_e \hat{c}}{2 \hat{\rho}} \left(\frac{\bar{V}_w}{M_w} - \frac{\bar{V}_e}{M_e} \right). \quad [12]$$

(To put Equation 11 in the form given, one must have that $\bar{V}_+ = (1 - t_+^w) \bar{V}_e$ and $\bar{V}_- = t_+^w \bar{V}_e$.²⁰) The law for the thermodynamic force on cations can be linearly transformed to produce a current/voltage relation:

$$\begin{aligned} \hat{\mathbf{i}} &= -\hat{\kappa}^{\text{eff}} \hat{\nabla} \hat{\phi} + \frac{2RT \hat{\chi} (1 - t_+^w) \hat{\kappa}^{\text{eff}}}{F \bar{V}_w \hat{c}_T} \hat{\nabla} \ln \hat{c} \\ &\quad + \frac{\hat{\kappa}^{\text{eff}}}{F \hat{c}} \left[\frac{M_+ \hat{c}}{\hat{\rho}} - \frac{2 \hat{\psi} (1 - t_+^w)}{\bar{V}_w \hat{c}_T} \right] \hat{\nabla} \hat{p}. \end{aligned} \quad [13]$$

Here $\hat{\kappa}^{\text{eff}}$ is the effective ionic conductivity; $\hat{\Phi}$ is the potential measured by a reversible hydrogen electrode at \hat{p} .²¹ Effective properties appear in Equations 11 and 13 because pore connectivity affects apparent transport rates. Letting \hat{D} and $\hat{\kappa}$ represent the diffusivity and conductivity of the pure liquid, we let

$$\hat{D}^{\text{eff}} = \hat{D}(\hat{\epsilon})\hat{\epsilon}^{3/2} \quad \text{and} \quad \hat{\kappa}^{\text{eff}} = \hat{\kappa}(\hat{\epsilon})\hat{\epsilon}^{3/2}, \quad [14]$$

following Bruggeman's tortuosity correlation.

The solid phase is electronically but not ionically conductive. Thus the current density there relates to the solid-phase potential, $\hat{\Phi}_s$, through Ohm's law,

$$\hat{\mathbf{i}}_s = -\sigma^{\text{eff}} \hat{\nabla} \hat{\Phi}_s, \quad [15]$$

where σ^{eff} is the effective electronic conductivity,

$$\sigma^{\text{eff}} = \sigma \hat{\epsilon}_s^{3/2}. \quad [16]$$

Here σ^{eff} is constant because $\hat{\epsilon}_s$, the volume fraction of nonreacting Pb bounded within electron-exchange surface \mathcal{A} , does not vary. Note that $\hat{\epsilon}_s$ does not count the volume fraction occupied by solid reactants, so $\hat{\epsilon}_s \neq 1 - \hat{\epsilon}$.

A constitutive law for liquid stress is needed to close the model.⁴ Below, terms involving momentum will be shown to be negligible in the first approximation. To analyze the scale of these terms, it will suffice to assume that current density induces a flow with low Reynolds number, in which case the homogenization of Cauchy's equation produces Darcy's law,

$$\hat{\mathbf{v}} = -\frac{\hat{\kappa}}{\hat{\mu}} \hat{\nabla} \hat{p}, \quad [17]$$

in which $\hat{\mu}$ is the liquid viscosity; pore geometry determines the Kozeny–Carman permeability $\hat{\kappa}$.

Interfacial constitutive laws.—Electrons are the only solid-phase charge carrier in Scheme 1, making interfacial electronic current a proxy for the half-reaction rates. No interfacial reactions occur in the separator domain, so $\hat{j} = 0$ uniformly there and the reactive area \mathcal{A} does not need to be defined there.

In an electrode subdomain where a single half-reaction involving n_e^- electrons occurs, the rate of change of the reaction extent is $\hat{j}/n_e - F$ and hence every \hat{S}_k is given by

$$\hat{S}_k = -\frac{s_k \hat{j}}{n_e - F}, \quad [18]$$

where s_k is the signed stoichiometric coefficient of species k in the half-reaction. (For a reduction half-reaction, s_k is positive for a product and negative for a reactant.)

Relationship 18 permits simpler expressions to be used in place of general material balances 6. First, Equations 5, 6, 7 and 18 combine to give

$$\hat{\nabla} \cdot \hat{\mathbf{v}}^\square = -\frac{\Delta \bar{V} \mathcal{A} j}{F}. \quad [19]$$

This liquid-phase volume balance introduces the volume of reaction $\Delta \bar{V}$, related to half-reaction stoichiometry by

$$n_e^- \Delta \bar{V} = \bar{V}_w s_w + \bar{V}_{-s_-} + \bar{V}_{+s_+} + \bar{V}_{\text{PbSO}_4} s_{\text{PbSO}_4} + \bar{V}_{\text{Pb}} s_{\text{Pb}} + \bar{V}_{\text{PbO}_2} s_{\text{PbO}_2}. \quad [20]$$

Second, one can combine Equations 2, 5, 6, 8, 11, 18, and 19 to show that the acid is governed by a form of the convective diffusion equation:

$$\frac{\partial}{\partial \hat{t}} (\hat{\epsilon} \hat{c}) + \hat{\mathbf{v}}^\square \cdot \hat{\nabla} \hat{c} = \hat{\nabla} \cdot \left[D^{\text{eff}} \left(\hat{\nabla} \hat{c} - \frac{\hat{\psi} \hat{\nabla} \hat{p}}{\hat{\chi} RT} \right) \right] + (s + \hat{c} \Delta \bar{V}) \frac{\mathcal{A} j}{F}. \quad [21]$$

The generation term here includes a single additional parameter,

$$s = -\frac{s_+ + n_e^- t_+^w}{n_e^-}. \quad [22]$$

Three aspects of acid-balance Equation 21 are new. First, the convection term, and second, the volume of reaction $\Delta \bar{V}$, appear because state Equation 3 imposes constraints on balances 6. Finally, a pressure-diffusion term appears because the flux laws are based on thermodynamic forces.

To complete the model, a chemical-kinetic constitutive law must be introduced to govern the local current density \hat{j} across pore surface \mathcal{A} . Generally such laws involve the voltage difference between the liquid and solid, the equilibrium potential of the half-reaction, and the chemical activities of the reactants. We assume the half-reactions in Scheme 1 are elementary, following Butler–Volmer kinetics. Butler–Volmer laws naturally include a symmetry factor, which we take to be one half,¹⁴ yielding

$$\hat{j} = 2 \hat{j}_0 \sinh \left(\frac{F \hat{\eta}}{RT} \right) + C_{\text{dl}} \frac{\partial (\hat{\Phi}_s - \hat{\Phi})}{\partial \hat{t}}, \quad [23]$$

where \hat{j}_0 is the concentration-dependent exchange-current density,

$$\hat{j}_0 = j^{\text{ref}} \left(\frac{\hat{c}}{c^{\text{ref}}} \right)^{\left| \frac{s_+}{n_e} \right| + \left| \frac{s_-}{n_e} \right|} \left(\frac{\hat{c}_w}{c_w^{\text{ref}}} \right)^{\left| \frac{s_w}{n_e} \right|}, \quad [24]$$

and $\hat{\eta}$ is the surface overpotential

$$\hat{\eta} = \hat{\Phi}_s - \hat{\Phi} - \hat{U}. \quad [25]$$

Here \hat{U} stands for the half-reaction's open-circuit potential (OCP) relative to a particular reference electrode. (The reference must be the same for all half-reactions.) Following Newmann and Tiedemann,¹² we use the formulas of Bode²² for the open-circuit potentials. Terms involving interfacial capacitance C_{dl} help to smooth out numerics, but have a negligible effect on model predictions because the capacitive time-scale is very short.²³

Equations 5, 8 to 10, and 13 to 25 comprise a three-dimensional model with closure at every interior point within an electrode pair.

Boundary conditions.—Symmetry and insulating boundary conditions demand that no species in the liquid phase flows through the centers, sides, and bottom of the electrode pair, so

$$\hat{\mathbf{N}}_+ \cdot \mathbf{n} = \hat{\mathbf{i}} \cdot \mathbf{n} = \hat{\mathbf{v}}^\square \cdot \mathbf{n} = 0 \quad \text{at } \hat{x} = 0, L, \hat{y} = 0, W \text{ and } \hat{z} = 0. \quad [26]$$

Kinematic relation 10 shows that $\hat{\mathbf{v}} \cdot \mathbf{n} = 0$ at these boundaries too. Flux laws 11, 13, and 17 further require the surface-normal gradients $\partial \hat{c} / \partial n$, $\partial \hat{p} / \partial n$ and $\partial \hat{\Phi} / \partial n$ to vanish at these boundaries.

Above the electrodes, there is a region of free electrolyte, with height $\hat{h}(\hat{t})$. At the top surface of this region, we impose a known external pressure \hat{p}_{ext} , and the absence of flux relative to the surface, which moves with velocity $\hat{\mathbf{v}}^{\text{head}} = (\partial \hat{h} / \partial \hat{t}) \mathbf{e}_z$:

$$(\hat{\mathbf{N}}_+ - \hat{\mathbf{v}}^{\text{head}} \hat{c}) \cdot \mathbf{n} = \hat{\mathbf{i}} \cdot \mathbf{n} = (\hat{\mathbf{v}}^\square - \hat{\mathbf{v}}^{\text{head}}) \cdot \mathbf{n} = 0,$$

$$\hat{p} = \hat{p}_{\text{ext}}, \quad \text{at } \hat{z} = H + \hat{h}(\hat{t}). \quad [27]$$

Note the final condition in Equation 27 determines the a priori unknown height $\hat{h}(\hat{t})$.

Hereafter, subscripts n and p denote property values in the negative- and positive-electrode subdomains. We choose the negative electrode to be the ground state, and define the cell voltage to be the potential at the positive electrode tab:

$$\hat{\Phi}_s = \begin{cases} 0 & \hat{\mathbf{x}} \in \text{tab}_n, \\ \hat{V}(\hat{t}) & \hat{\mathbf{x}} \in \text{tab}_p. \end{cases} \quad [28]$$

One can either control the voltage, or consider a current-controlled discharge where the voltage is determined by

$$-\int_{\text{tab}_n} \hat{\mathbf{i}}_s \cdot \mathbf{n} dS = \int_{\text{tab}_p} \hat{\mathbf{i}}_s \cdot \mathbf{n} dS = \hat{I}_{\text{circuit}}(\hat{t})/8, \quad [29]$$

where \hat{I}_{circuit} is the current drawn from the battery, which is positive for a discharge; the factor of 8 appears because the cell comprises eight electrode pairs in parallel.

This paper focuses on experiments under ‘galvanic control’, following condition 29, which allow $\hat{I}_{\text{circuit}}(\hat{t})$ to be any function of time. Since six cells are connected in series, the voltage in the external circuit is $\hat{V}_{\text{circuit}} = 6\hat{V}$.

Relationships between subdomains.—The liquid phase permeates all three subdomains. Therefore scalar variables \hat{c} , \hat{p} , and $\hat{\Phi}$, as well as the normal components of all the flux vectors, are continuous across electrode/separators boundaries.

There is no solid-phase current across the boundary of the separator subdomain, nor is there any pore-surface charge exchange within it, so \hat{i}_s vanishes uniformly there. Further, since the separator subdomain electronically isolates the positive and negative electrodes, $\hat{\Phi}_s$ is not continuous across it.

Integrating the interfacial current distributions in Equation 9 and applying the divergence theorem, boundary conditions 29 and the fact that \hat{i}_s vanishes at the electrode/separators interfaces lead to integral constraints,

$$\int_0^H \int_0^W \int_0^{l_n} \mathcal{A}_n \hat{j}_n \, d\hat{x} d\hat{y} d\hat{z} = - \int_0^H \int_0^W \int_{L-l_p}^L \mathcal{A}_p \hat{j}_p \, d\hat{x} d\hat{y} d\hat{z} = \hat{I}_{\text{circuit}}/8. \quad [30]$$

In short, these say that the total current leaving the negative electrode domain must enter the positive electrode domain. Equation 30 will help to assess the scales of pressure and velocity in the Dimensionless model section.

Initial conditions.—The initial electrolyte concentration and electrode porosities are spatially uniform, but depend on the state of charge, q , which we define as

$$q = q^0 - \frac{1}{q^{\max}} \int_0^{\hat{t}} \hat{I}_{\text{circuit}}(s) \, ds. \quad [31]$$

Let c^{\max} , ϵ_n^{\max} and ϵ_p^{\max} be the values of electrolyte concentration, negative electrode porosity, and positive electrode porosity, respectively, at full state of charge. In a lead-acid battery, the state of charge is closely linked to the concentration of the electrolyte. Hence q is chosen to be unity when the concentration of the electrolyte is at its maximum value, c^{\max} , and zero when the concentration of the electrolyte is zero, so that the initial conditions are

$$\hat{c} = \hat{c}^0 = c^{\max} q^0, \quad \hat{\epsilon} = \hat{\epsilon}^0 = \epsilon^{\max} - \epsilon^{\Delta}(1 - q^0) \quad \text{at } \hat{t} = 0. \quad [32]$$

Parameters q^{\max} and ϵ^{Δ} are chosen to make Equations 31 and 32 consistent with Equations 5 and 21 (see Appendix A for details):

$$q^{\max} = \frac{8FA_{\text{cs}}(l_n \epsilon_n^{\max} + l_{\text{sep}} \epsilon_{\text{sep}}^{\max} + l_p \epsilon_p^{\max}) c^{\max}}{s_p - s_n}, \quad [33]$$

$$\epsilon^{\Delta} = \frac{\Delta \bar{V}_{\text{surf}} q^{\max}}{16FA_{\text{cs}} l}. \quad [34]$$

Finally, because interfacial capacitance effects are included, initial conditions are needed for the potentials; we choose spatially homogeneous values, letting

$$\hat{\Phi} = -\hat{U}_{\text{pb}}(\hat{c}^0) \quad \text{and} \quad [35a]$$

$$\hat{\Phi}_s = \begin{cases} 0, & 0 < \hat{x} < l_n \\ \hat{U}_{\text{pbO}_2}(\hat{c}^0) - \hat{U}_{\text{pb}}(\hat{c}^0), & L - l_p < \hat{x} < L \end{cases} \quad [35b]$$

so that $\hat{j} = 0$ everywhere at $\hat{t} = 0$.

Dimensionless model.—Nondimensionalization of the model presented above helps to determine the dominant physical phenomena in the system. If $\partial \hat{h}/\partial \hat{t}$ is sufficiently small and the electrode conductivity is sufficiently high, one can assume uniformity in the plane normal to \hat{x} , reducing the problem to one spatial dimension. In this case, the

current density is uniform in the current collectors at $\hat{x} = 0$ and $\hat{x} = L$, and so boundary condition 29 becomes

$$\hat{\mathbf{i}}_s \cdot \mathbf{e}_x = \hat{i}_{\text{cell}}(\hat{t}) = \hat{I}_{\text{circuit}}/8A_{\text{cs}} \quad \text{at } \hat{x} = 0, L, \quad [36]$$

which introduces the variable \hat{i}_{cell} to stand for the total current density at the cell level. Let \hat{N}_+ , \hat{i}_+ , \hat{i}_s , \hat{v}^{\square} and \hat{v} represent the \hat{x} -components of vectors $\hat{\mathbf{N}}_+$, $\hat{\mathbf{i}}_+$, $\hat{\mathbf{i}}_s$, $\hat{\mathbf{v}}^{\square}$ and $\hat{\mathbf{v}}$. A first set of dimensionless variables is formed by the natural rescalings

$$x = \hat{x}/L, \quad (i, i_s) = (\hat{i}, \hat{i}_s)/\bar{i}, \quad c = \hat{c}/c^{\max}, \quad \epsilon = \hat{\epsilon}, \quad [37a]$$

where $\bar{i} = \max_{\hat{t}}(\hat{i}_{\text{cell}}(\hat{t}))$.

Reduce the number of parameters by identifying the scale of interfacial current density, \bar{i}/AL , and discharge time-scale, $c^{\max} FL/\bar{i}$. Hence nondimensionalize interfacial current density, exchange-current density, and time as

$$(j_n, j_{0,n}) = (\hat{j}_n, \hat{j}_{0,n}) \left/ \frac{\bar{i}}{A_n L} \right., \quad [37b]$$

$$(j_p, j_{0,p}) = (\hat{j}_p, \hat{j}_{0,p}) \left/ \frac{\bar{i}}{A_p L} \right., \quad [37c]$$

$$t = \hat{t} \left/ \frac{c^{\max} FL}{\bar{i}} \right. \quad [37d]$$

After nondimensionalization, $j_{0,n}$ and $j_{0,p}$ become $\mathcal{O}(1)$ functions. To nondimensionalize the potentials, note that the dominant exponents in the hyperbolic-sine terms of Equation 23 should be $\mathcal{O}(1)$, since the terms multiplying the sinh functions are all $\mathcal{O}(1)$. Equation A1 can be exploited to define dimensionless open-circuit potentials

$$U_{\text{pb}}(c) = \frac{F}{RT} (\hat{U}_{\text{pb}}(\hat{c}) - U_{\text{pb}}^{\ominus}) \quad \text{and} \quad [38a]$$

$$U_{\text{pbO}_2}(c) = \frac{F}{RT} (\hat{U}_{\text{pbO}_2}(\hat{c}) - U_{\text{pbO}_2}^{\ominus}). \quad [38b]$$

Then, to ensure that the exponents in Equation 23 are $\mathcal{O}(1)$ and noting that $\hat{\Phi}_s = 0$ at $\hat{x} = 0$, introduce the dimensionless potentials

$$\Phi = \frac{F}{RT} (\hat{\Phi} + U_{\text{pb}}^{\ominus}), \quad [39a]$$

$$\Phi_s = \begin{cases} \frac{F}{RT} \hat{\Phi}_s, & 0 < \hat{x} < l_n \\ \frac{F}{RT} (\hat{\Phi}_s - U_{\text{pbO}_2}^{\ominus} + U_{\text{pb}}^{\ominus}), & L - l_p < \hat{x} < L. \end{cases} \quad [39b]$$

Quantities \hat{D} (and hence \hat{D}^{eff}) and \hat{c}_w are appropriately scaled with their values at $c = c^{\max}$:

$$D(c) = \hat{D}(\hat{c})/\hat{D}^{\max}, \quad c_w(c) = \hat{c}_w(\hat{c})/\hat{c}_w^{\max}, \quad [40]$$

where $\hat{D}^{\max} = \hat{D}(c^{\max})$ and $\hat{c}_w^{\max} = \hat{c}_w(c^{\max})$. The ionic conductivity and Darken thermodynamic factor rescale as

$$\kappa(c) = \frac{RT \hat{\kappa}(\hat{c})}{F^2 \hat{D}^{\max} c^{\max}}, \quad \chi(c) = \frac{2(1 - t_+^w) \hat{\chi}(\hat{c})}{1 - \alpha c}, \quad [41]$$

where the quantity $\alpha = -(2\bar{V}_w - \bar{V}_e)c^{\max}$ is the excluded-volume number defined by Liu and Monro. ⁴

In Equation 24 for the exchange-current density, the reference concentrations are taken to be $\hat{c}^{\text{ref}} = \hat{c}^{\max}$ and $\hat{c}_w^{\text{ref}} = \hat{c}_w^{\max}$. The dimensionless widths of the negative electrode, separator and positive electrode become $\ell_n = l_n/L$, $\ell_{\text{sep}} = l_{\text{sep}}/L$, and $\ell_p = l_p/L$, respectively.

In velocity Equations 10, 17 and 19, \hat{p} and $\hat{\mu}$ are scaled with their values at c^{\max} , and $\hat{\mathcal{K}}$, with d^2 , where d is the characteristic pore size at full charge. The reaction velocity scale is $v^{\text{rxn}} = \bar{i}/c^{\max} F$, and the Darcy pressure scale $\mu^{\max} v^{\text{rxn}} L/d^2$, so that

$$(v^{\square}, v) = (\hat{v}^{\square}, \hat{v}) \left/ \frac{\bar{i}}{c^{\max} F} \right., \quad [42a]$$

$$p = (\hat{p} - p^{\text{ref}}) \left/ \frac{\mu^{\max} v^{\text{rxn}} L}{d^2} \right., \quad [42b]$$

Table I. Dimensionless parameters, relative to the C-rate, $\mathcal{C} = 8A_{cs}\bar{i}/Q$. \mathcal{C}_d is the diffusional C-rate.

| Parameter | Definition | Interpretation | Value | | |
|-----------------------|---|--|----------------------------------|--------------------|----------------------|
| | | | n | sep | p |
| \mathcal{C}_d | $\frac{\bar{i}}{c^{\max} D^{\max} F/L}$ | applied current density limiting current density | | 0.60 \mathcal{C} | |
| ι_s | $\frac{\sigma^{\text{eff}} RT/FL}{\bar{i}}$ | ohmic current scale applied current density | $3.8 \times 10^4/\mathcal{C}$ | - | 55/ \mathcal{C} |
| β^{surf} | $-\frac{c^{\max}}{n_e^-} \sum_{k \in \{\text{PbSO}_4, \text{Pb}, \text{PbO}_2\}} \bar{V}_k s_k$ | Change in porosity associated with local half-reaction going to completion | 0.084 | - | -0.064 |
| β | $-\frac{c^{\max}}{\Delta \bar{V}}$ | Change in acid volume fraction associated with local half-reaction going to completion | 0.033 | - | 0.040 |
| γ_{dl} | $\frac{C_{\text{dl}} RT AL/F \bar{i}}{c^{\max} FL/\bar{i}}$ | capacitance time-scale discharge time-scale | 2.1×10^{-5} | - | 1.7×10^{-4} |
| ω_c | $\frac{c^{\max} M_e}{\rho^{\max}} \left(1 - \frac{M_w \bar{V}_e}{M_e \bar{V}_w} \right)$ | Diffusive kinematic relationship coefficient | 0.70 | | |
| ω_i | $\frac{c^{\max} M_e}{\rho^{\max}} \left(\iota_w + \frac{M_-}{M_e} \right)$ | Migrative kinematic relationship coefficient | 0.41 | | |
| π_{os} | $\frac{\mu^{\max} v^{\text{rxn}} L/d^2}{RT c^{\max}}$ | viscous pressure scale osmotic pressure scale | $3.6 \times 10^{-5} \mathcal{C}$ | | |

where p^{ref} is a reference pressure (e.g. atmospheric). This scaling transforms the equations governing v^{\square} , v and p to

$$\frac{\partial v^{\square}}{\partial x} = \beta j, \quad [43a]$$

$$v = -\frac{\mathcal{K}}{\mu} \frac{\partial p}{\partial x}, \quad [43b]$$

$$\rho(v - v^{\square}) = -\frac{\omega_c}{\mathcal{C}_d} D^{\text{eff}} \frac{\partial c}{\partial x} + \omega_i i, \quad [43c]$$

in which the dimensionless parameters β , ω_c and ω_i are defined in Table I. Further, the effect of pressure gradients in Equations 13 and 21 is smaller than the effect of concentration gradients (ignoring the $\mathcal{O}(1)$ functions of concentration χ and ψ) by a factor of

$$\pi_{\text{os}} = \frac{\mu^{\max} v^{\text{rxn}} L}{d^2 RT c^{\max}}. \quad [44]$$

Since β takes different values in the two electrodes, Equation 43a does not admit a one-dimensional solution where v^{\square} vanishes at both electrode centers (see Appendix B). That is, the y - and/or z -component of v^{\square} must be non-zero, and there must be a flow in the directions normal to the x -axis. In order to systematically account for this inherently three-dimensional nature of velocity in a one-dimensional model, one must conduct a detailed analysis of the three-dimensional model. Our preliminary analysis of the higher-dimensional problem suggests that the distributions of the normal components of v^{\square} depend strongly on geometric properties of the battery, such as relative porosities in different domains and aspect ratio of the cell sandwich. Such analysis is beyond the scope of this paper; the limit of finite β will be addressed in a future study.

At present, we note that the dimensionless parameters β and π_{os} are very small, and therefore assume a limit where both of these parameters are zero (and hence $\partial \hat{h}/\partial \hat{t} = 0$), in which case v^{\square} vanishes everywhere, and v and p decouple from the other variables. The resulting one-dimensional full model can then be solved to find the voltage without needing the velocity and pressure.

Having decoupled flow velocity and pressure from the rest of the model, the following dimensionless system for c , j , ε , i , Φ , i_s and Φ_s results:

$$\frac{\partial}{\partial t}(\varepsilon c) = \frac{1}{\mathcal{C}_d} \frac{\partial}{\partial x} \left(D^{\text{eff}} \frac{\partial c}{\partial x} \right) + s j, \quad [45a]$$

$$\frac{\partial \varepsilon}{\partial t} = -\beta^{\text{surf}} j, \quad [45b]$$

$$\frac{\partial i}{\partial x} = j, \quad [45c]$$

$$\mathcal{C}_d i = \kappa^{\text{eff}} \left(\chi \frac{\partial \ln(c)}{\partial x} - \frac{\partial \Phi}{\partial x} \right), \quad [45d]$$

$$\frac{\partial i_s}{\partial x} = -j, \quad [45e]$$

$$i_s = -\iota_s \frac{\partial \Phi_s}{\partial x}, \quad [45f]$$

$$j = 2j_0 \sinh(\Phi_s - \Phi - U(c)) + \gamma_{\text{dl}} \frac{\partial}{\partial t}(\Phi_s - \Phi), \quad [45g]$$

with boundary conditions

$$\Phi_s = \frac{\partial c}{\partial x} = i = 0, \quad i_s = i_{\text{cell}} \quad \text{at } x = 0, 1, \quad [45h]$$

$$i_s = 0 \quad \text{at } x = \ell_n, 1 - \ell_p, \quad [45i]$$

and initial conditions

$$c = q^0, \quad [45j]$$

$$\varepsilon = \varepsilon^{\max} - \varepsilon^{\Delta}(1 - q^0), \quad [45k]$$

$$\Phi = -U_{\text{Pb}}(q^0), \quad [45l]$$

$$\Phi_s = \begin{cases} 0, & 0 < x < \ell_n \\ U_{\text{PbO}_2}(c^0) - U_{\text{Pb}}(c^0), & 1 - \ell_p < x < 1. \end{cases} \quad [45m]$$

Integral condition 30 nondimensionalizes to

$$\int_0^{\ell_n} j_n \, d\hat{x} = - \int_{1-\ell_p}^1 j_p \, d\hat{x} = i_{\text{cell}}. \quad [45n]$$

Composition dependences of the properties D^{eff} , χ , κ^{eff} , j_0 , U_{Pb} , and U_{PbO_2} are established through the functions listed in Table AII. The four dominant dimensionless parameters, \mathcal{C}_d , ι_s , β^{surf} and γ_{dl} , are defined in Table I, which also states physical interpretations and typical values. In particular, the diffusional C-rate can be written as

$$\mathcal{C}_d = L^2/D^{\max} \times \frac{Q}{8A_{cs} c^{\max} FL} \times \frac{8A_{cs} \bar{i}}{Q}, \quad [46]$$

where $8A_{cs} c^{\max} FL$ is the volumetric capacity of the battery (in Ah), Q is the capacity of the battery (in Ah), and $\mathcal{C} = 8A_{cs} \bar{i}/Q$ is the C-rate of operation. Alternatively, one can identify \mathcal{C}_d to be the ratio between the applied current scale, \bar{i} , and the scale of the liquid-phase limiting current, $i_L = c^{\max} D^{\max} F/L$.

In the Results section, q^0 will be taken to be unity (the battery starts from a fully charged state) unless explicitly stated.

Numerical Solution

The system of Equations 45 was solved numerically. Code used to solve the model and generate the results below is available publicly on GitHub.²⁴

To facilitate numerical solution, the model was first manipulated into a form suitable for application of the Finite Volume Method. Letting $\phi = \Phi_s - \Phi$ and noting that $i_s = i_{\text{cell}} - i$, one can replace Equations 45d to 45f with

$$C_d i = \kappa^{\text{eff}} \left(\chi \frac{\partial \ln(c)}{\partial x} - \frac{\partial \Phi}{\partial x} \right), \quad [47a]$$

$$i_{\text{cell}} - i = -\iota_s \frac{\partial}{\partial x} (\phi + \Phi). \quad [47b]$$

We also eliminate $\partial \Phi / \partial x$ from Equation 47 to find i as a functional of c and ϕ :

$$i = \kappa^{\text{eff}} \frac{\chi \frac{\partial \ln(c)}{\partial x} + \frac{\partial \phi}{\partial x} + i_{\text{cell}} / \iota_s}{C_d + \kappa^{\text{eff}} / \iota_s}. \quad [48a]$$

The result is a closed system of partial differential equations for c , ε and ϕ :

$$\frac{\partial}{\partial t} (\varepsilon c) = \frac{1}{C_d} \frac{\partial}{\partial x} \left(D^{\text{eff}} \frac{\partial c}{\partial x} \right) + s j, \quad [48b]$$

$$\frac{\partial \varepsilon}{\partial t} = -\beta^{\text{surf}} j, \quad [48c]$$

$$\frac{\partial \phi}{\partial t} = \frac{1}{\gamma_{\text{dl}}} (j - 2 j_0 \sinh [\phi - U]), \quad [48d]$$

where $j = \partial i / \partial x$ is obtained by differentiating Equation 48a in each electrode and vanishes in the separator, with boundary conditions

$$\frac{\partial c}{\partial x} = i = 0 \quad \text{at } x = 0, 1, \quad [48e]$$

$$i = i_{\text{cell}} \quad \text{at } x = \ell_n, 1 - \ell_p, \quad [48f]$$

and initial conditions derived from Equation 45j.

Equation system 48 is solved by discretising the spatial domain using Finite Volumes, choosing the spatial discretisation to be uniform within each subdomain and as uniform as possible across subdomains (100 points in the negative electrode, 170 in the separator, and 140 in the positive electrode were deemed sufficient). The results are robust to the total number of points chosen; 410 were chosen here to achieve grid independence in one minute.

Having discretized in space, the resulting system of transient ordinary differential equations is solved using `scipy.integrate` in Python.²⁵ Finally, Φ is calculated as

$$\Phi = \int_0^x \left(\chi \frac{\partial \ln(c)}{\partial x} - C_d \frac{i}{\kappa^{\text{eff}}} \right) dx - \phi|_{x=0}, \quad [48g]$$

where the final term comes from the fact that $\Phi = -\phi$ at $x = 0$. The voltage drop across the electrode pair is computed with

$$V = \Phi_s|_{x=1} = (\phi + \Phi)|_{x=1}. \quad [48h]$$

Crucially, the partial differential equation system 48 is much easier to solve than the differential-algebraic system 45.

Results

Figure 2 shows the (dimensional) voltage against capacity used for a range of C-rates. As is to be expected, the total capacity available decreases as the C-rate increases. This dependence is further elucidated by exploring the total capacity of the battery for constant-current discharges across a higher range of C-rates, summarized on Figure 3. By Peukert's Law, one would expect the graph to be linear on this

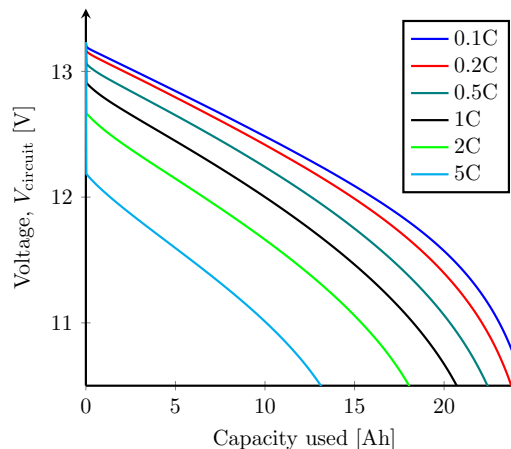


Figure 2. Comparing voltages for a constant-current discharge using the parameters from literature (Table AI), for a range of C-rates.

log-log plot. However, in this case deviations from linearity occur because there are two distinct capacity-limiting mechanisms. At low C-rates (below 1C), the battery capacity is concentration-limited, with full discharge occurring when the electrolyte concentration reaches zero. At high C-rates, the battery is voltage-limited, because the cut-off voltage of 10.5V is achieved before the bulk concentration falls to zero.

The model also allows internal variables to be explored, particularly the local water concentration. Electrolyte and water concentrations are depicted in Figure 4. At a very low C-rate of 0.1C (Figure 4a), both concentrations remain almost uniform throughout the discharge; electrolyte concentration decreases, and water concentration increases proportionally. At higher C-rates of 0.5C (Figure 4b) and 2C (Figure 4c), the concentrations become spatially inhomogeneous, which leads to concentration overpotentials that limit the accessible capacity.

A Derivative-Free Gauss-Newton method²⁶ was used to fit the model to data from a series of constant-current discharges of a 17 Ah BBOXX Solar Home battery at intervals of 0.5 A from 3 A to 0.5 A (Figure 5). Each constant-current discharge was followed by a two-hour rest period at open circuit (zero current). The model yields a good fit to the data, with a root-mean-square error of 43 mV, but this approach is slow since it requires solving the full system of partial differential equations at each iteration. A faster approach will be developed in part II.⁵

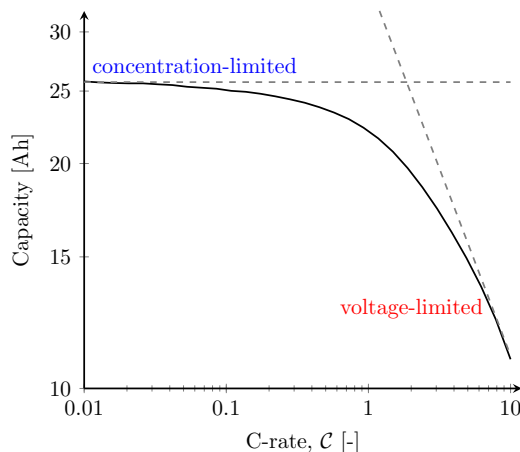


Figure 3. Log-log plot of battery capacity against C-rate, using the parameters from literature (Table AI). Dashed lines indicate the expected behavior from Peukert's law.

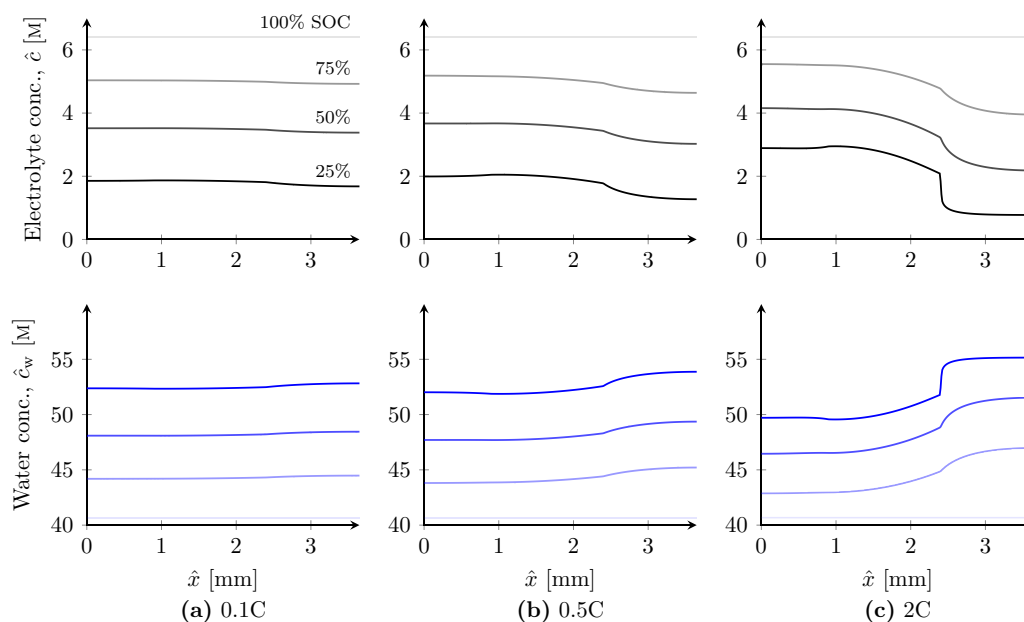


Figure 4. Electrolyte and water concentrations at various States of Charge (SOCs) for a constant-current discharge using the parameters from literature (Table AI), for a range of C-rates. Opacity increases with decreasing SOC.

Conclusions

Three novel phenomena were included in a porous-electrode model for lead-acid batteries. First, the mass-averaged and volume-averaged velocities of the electrolyte were both considered, the former associated with momentum transport and the latter with kinematics. Due to density variation in the liquid, and volume changes associated with the electrode reactions, neither of these velocities remains solenoidal after homogenisation. Second, an extra convective term, associated with the volume-averaged velocity, drives cation transport. Third, a pressure-diffusion term drives cation transport, and appears also in the MacInnes equation (modified Ohm's law) describing the liquid. Although these terms are small in magnitude for lead-acid batteries discharged at low-to-moderate rates, they could be important for other chemistries where large volume changes occur during charge/discharge, such as lithium-ion batteries with silicon anodes,^{27–32} or to understand other scenarios such as the impedance signature of electromechanical/transport coupling.³³ Nondimensionalization of this model led to the identi-

cation of key parameter groupings, a methodology that could extend easily to other models and chemistries.

Two distinct mechanisms determine the total cell capacity: concentration limitation at low C-rates, and voltage limitation at high C-rates. In addition to concentration limitation and voltage limitation, capacity could be limited by additional physical effects, such as pore occlusion at very high C-rates.¹⁸

The model developed in this paper provides physical detail about the electrochemical processes occurring in a lead-acid battery during discharge, but is ultimately too computationally intensive to underpin an advanced battery management system. In part II,⁵ asymptotic analysis is used to derive three simplified models valid at low-to-moderate discharge rates. These can be solved much faster than the detailed model developed here, while giving more physical insight than an equivalent circuit.

Acknowledgments

This publication is based on work supported by the EPSRC center For Doctoral Training in Industrially Focused Mathematical Modelling (EP/L015803/1) in collaboration with BBOX. JC, CP, DH and CM acknowledge funding from the Faraday Institution (EP/S003053/1).

List of Symbols

We list below the variables in the model. Parameters and functions are given in Tables AI and AII respectively.

Variables

| | | |
|---------------|--------------------------------|-----------------------------------|
| c | concentration | mol m^{-3} |
| ε | porosity | - |
| j | interfacial current density | A m^{-2} |
| \mathbf{i} | current density (3D) | A m^{-2} |
| i | current density in x-direction | A m^{-2} |
| \mathbf{v} | velocity (3D) | m s^{-1} |
| v | velocity in x-direction | m s^{-1} |
| \mathbf{N} | ion flux (3D) | $\text{mol m}^{-2} \text{s}^{-1}$ |
| p | pressure | Pa |
| Φ | potential | V |

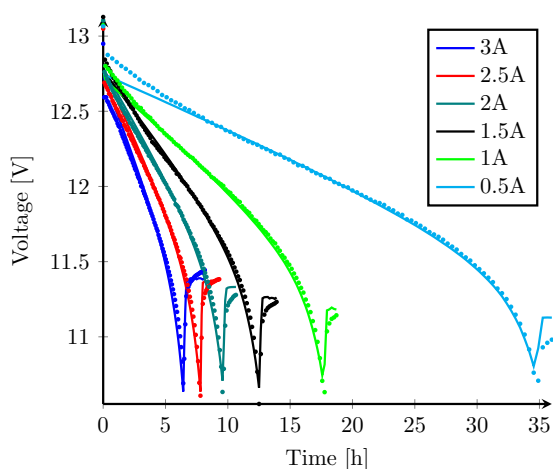


Figure 5. Comparing data (dots) with results from full numerical model (lines) for a range of currents, with parameters fitted using DFO-GN. The root-mean-square-error of the fit is 43 mV.

| Subscripts | |
|------------|-----------------------|
| n | in negative electrode |
| sep | in separator |
| p | in positive electrode |
| + | of cations |
| − | of anions |
| w | of solvent (water) |
| e | of electrolyte |
| s | of solid (electrodes) |

| Superscripts | |
|--------------|-----------------|
| 0 | initial |
| max | maximum |
| eff | effective |
| surf | surface |
| □ | volume-averaged |

| Accents | |
|---------|--------|
| ˆ | scaled |

Appendix A. Parameters

The dimensional parameters are given in Table AI, and the concentration dependences of coefficients are laid out in Table AII. Formulae for open-circuit potentials were obtained empirically by Bode.²² Note that these could be written as

$$\hat{U}_{\text{Pb}}(\hat{c}) = U_{\text{Pb}}^{\ominus} + \frac{RT}{F} U_{\text{Pb}}(c), \quad [\text{A1a}]$$

$$\hat{U}_{\text{PbO}_2}(\hat{c}) = U_{\text{PbO}_2}^{\ominus} + \frac{RT}{F} U_{\text{PbO}_2}(c), \quad [\text{A1b}]$$

to reflect their relation to the Nernst equation (following Treptow³⁴), with $U_{\text{Pb}}^{\ominus} = -0.295$ and $U_{\text{PbO}_2}^{\ominus} = 1.628$.

Consistent initial conditions.—For consistent initial conditions, we take ‘starting at $x\%$ SOC’ to mean an internally equilibrated (i.e. spatially homogeneous) initial state at uniform concentration corresponding to this charge. The following determines initial conditions for \hat{c} and $\hat{\epsilon}$ consistent with this choice.

Considering a one-dimensional model and integrating Equation 21 in \hat{x} across the whole electrode pair and using the no-flux conditions 26, and the integral condition 30,

$$\int_0^L (\hat{\epsilon} \hat{c}) d\hat{x} = A_{\text{cs}} \left(l_n \epsilon_n^{\text{max}} + l_{\text{sep}} \epsilon_{\text{sep}}^{\text{max}} + l_p \epsilon_p^{\text{max}} \right) c^{\text{max}} + \frac{(s_n - s_p) q^{\text{max}} (1 - q)}{8F}. \quad [\text{A2}]$$

Both sides of Equation A2 should be zero when $q = 0$; hence choose

$$q^{\text{max}} = \frac{8FA_{\text{cs}} \left(l_n \epsilon_n^{\text{max}} + l_{\text{sep}} \epsilon_{\text{sep}}^{\text{max}} + l_p \epsilon_p^{\text{max}} \right) c^{\text{max}}}{s_p - s_n}, \quad [\text{A3}]$$

which, with the parameter values in Table AI, gives a maximum capacity of 26.1 Ah for the battery. This compares favorably to the stated battery capacity of 17 Ah.

Now, integrating Equation 5 in \hat{x} across the whole negative electrode and using the integral condition 30,

$$\int_0^{l_n} \hat{\epsilon}_n d\hat{x} = A_{\text{cs}} l_n \epsilon_n^{\text{max}} + \frac{\Delta \bar{V}_n^{\text{surf}} q^{\text{max}} (1 - q)}{16F}. \quad [\text{A4}]$$

Then, assuming that ϵ_n^0 is spatially uniform,

$$\epsilon_n^0 = \epsilon_n^{\text{max}} - \epsilon_n^{\Delta} (1 - q^0), \quad \text{where} \quad \epsilon_n^{\Delta} = \frac{\Delta \bar{V}_n^{\text{surf}} q^{\text{max}}}{16FA_{\text{cs}} l_n}. \quad [\text{A5}]$$

Similarly,

$$\epsilon_p^0 = \epsilon_p^{\text{max}} - \epsilon_p^{\Delta} (1 - q^0), \quad \text{where} \quad \epsilon_p^{\Delta} = \frac{\Delta \bar{V}_p^{\text{surf}} q^{\text{max}}}{16FA_{\text{cs}} l_p}. \quad [\text{A6}]$$

Appendix B. Velocity

Integrating Equation 43a for the volume-averaged velocity from $x = 0$ to $x = 1$, and using integral condition 30 for the interfacial current density and Equation 45h for v^{\square} at $x = 0$, one finds that

$$v^{\square} \Big|_{x=1} = (\beta_n - \beta_p) i_{\text{cell}}, \quad [\text{B1}]$$

Table AI. Dimensional parameters from the literature. Parameters with several values indicate different values in negative electrode (n), separator (s) and positive electrode (p). (*) Reported by .¹⁴ P.M.V. = Partial Molar Volume.

| Parameter | Name | Value | | | Units | Refs. |
|---------------------------|-----------------------------------|----------------------|-----------------------|-----------------------|-----------------------------------|----------|
| | | n | sep | p | | |
| l | Subdomain width | 0.9×10^{-3} | 1.5×10^{-3} | 1.25×10^{-3} | m | 36 |
| ϵ^{max} | Electrode porosity | 0.53 | 0.92 | 0.57 | - | 23 |
| H | Battery height | | 11.4×10^{-2} | | m | Measured |
| W | Battery depth | | 6.5×10^{-2} | | m | Measured |
| s_+ | Stoichiometry of cations | −1 | - | −3 | - | 1 |
| s_- | Stoichiometry of anions | 1 | - | −1 | - | 1 |
| s_w | Stoichiometry of Water | 0 | - | 2 | - | 1 |
| n_e | Number of electrons | 2 | - | 2 | - | 1 |
| \bar{V}_w | P.M.V. of water | | 1.75×10^{-5} | | $\text{m}^3 \text{mol}^{-1}$ | 10 |
| \bar{V}_+ | P.M.V. of cations | | 1.35×10^{-5} | | $\text{m}^3 \text{mol}^{-1}$ | 35 |
| \bar{V}_- | P.M.V. of anions | | 3.15×10^{-5} | | $\text{m}^3 \text{mol}^{-1}$ | 35 |
| \bar{V}_{Pb} | P.M.V. of lead | | 1.83×10^{-5} | | $\text{m}^3 \text{mol}^{-1}$ | 37 |
| \bar{V}_{PbO_2} | P.M.V. of lead dioxide | | 2.55×10^{-5} | | $\text{m}^3 \text{mol}^{-1}$ | 37 |
| \bar{V}_{PbSO_4} | P.M.V. of lead sulfate | | 4.82×10^{-5} | | $\text{m}^3 \text{mol}^{-1}$ | 37 |
| M_w | Molar mass of water | | 1.8×10^{-2} | | kg mol^{-1} | 37 |
| M_+ | Molar mass of cations | | 0.1×10^{-2} | | kg mol^{-1} | 37 |
| M_- | Molar mass of anions | | 9.7×10^{-2} | | kg mol^{-1} | 37 |
| F | Faraday constant | | 96485 | | C mol^{-1} | - |
| R | Ideal gas constant | | 8.314 | | $\text{J mol}^{-1} \text{K}^{-1}$ | - |
| T | Room temperature | | 298.15 | | K | - |
| t_+^w | Transference number | | 0.72 | | - | 14,17 |
| σ | Solid conductivity | 4.8×10^6 | - | 8×10^4 | S m^{-1} | 15 |
| j^{ref} | Reference exchange-current | 8×10^{-2} | - | 6×10^{-3} | A m^{-2} | 38 (*) |
| c^{max} | Initial electrolyte concentration | | 5.6×10^3 | | mol m^{-3} | 36 |
| \mathcal{A} | Surface area per volume | 2.6×10^6 | - | 2.05×10^7 | m^{-1} | 38 (*) |
| d | Pore size at full charge | 10^{-7} | - | 10^{-7} | m | 15 |
| C_{dl} | Double-layer capacity | 0.2 | - | 0.2 | F m^{-2} | 23 |
| q^0 | Full initial SOC | | 1 | | - | - |
| Q | Manufacturer-specified capacity | | 17 | | Ah | - |

Table AII. Dimensional functions of concentration, \hat{c} (measured in mol/m³) and $\hat{\varepsilon}$ (dimensionless). (†) Empirical formulae are given by Gu et al.,¹⁵ citing Tiedemann and Newman,³⁸ and agree with data from Chapman and Newman.¹⁷ (*) Our fit to data of given reference(s). (‡) Molality m is defined as $m(\hat{c}) = \hat{c}\bar{V}_w / [(1 - \hat{c}\bar{V}_e)M_w]$.

| Function | Name | Formula | Value at $\hat{c} = c^{\max}$ | Units | Refs. |
|--------------------------|------------------------------|---|-------------------------------|--------------------------------|-----------|
| \hat{D} | Electrolyte diffusivity | $(1.75 + 2.6 \times 10^{-4}\hat{c}) \times 10^{-9}$ | 3.02×10^{-9} | m ² s ⁻¹ | (†) |
| $\hat{\chi}$ | Thermodynamic factor | $0.49 + 4.1 \times 10^{-4}\hat{c}$ | 2.8 | - | 17,39 (*) |
| $\hat{\kappa}$ | Electrolyte conductivity | $\hat{c} \exp(6.23 - 1.34 \times 10^{-4}\hat{c} - 1.61 \times 10^{-8}\hat{c}^2) \times 10^{-4}$ | 77 | S m ⁻¹ | (†) |
| $\hat{\rho}$ | Electrolyte density | $M_w/\bar{V}_w (1 + (M_e\bar{V}_w/M_w - \bar{V}_e)\hat{c})$ | 1.32×10^3 | kg m ⁻³ | 40 |
| $\hat{\mathcal{K}}$ | Permeability | $\hat{\varepsilon}^3 d^2 / 180(1 - \hat{\varepsilon})^2$ | - | m ² | 15 |
| $\hat{\mu}$ | Electrolyte viscosity | $0.89 \times 10^{-3} + 1.11 \times 10^{-7}\hat{c} + 3.29 \times 10^{-11}\hat{c}^2$ | 2.5×10^{-3} | Pa s | 17 (*) |
| \hat{c}_w | Water concentration | $(1 - \hat{c}\bar{V}_e)/\bar{V}_w$ | 4.27×10^4 | mol m ⁻³ | 3 |
| \hat{j}_0 | Exchange-current density | $j^{\text{ref}} \left(\frac{\hat{c}}{c^{\text{ref}}} \right)^{\left \frac{s_+}{n_e} \right + \left \frac{s_-}{n_e} \right } \left(\frac{\hat{c}_w}{c_w^{\text{ref}}} \right)^{\left \frac{s_w}{n_e} \right }$ | j^{ref} | A m ⁻² | 18 |
| \hat{U}_{Pb} | Open-circuit potential (neg) | $-0.295 - 0.074 \log m - 0.030 \log^2 m - 0.031 \log^3 m - 0.012 \log^4 m$ (‡) | -0.41 | V | 22 |
| \hat{U}_{PbO_2} | Open-circuit potential (pos) | $1.628 + 0.074 \log m + 0.033 \log^2 m + 0.043 \log^3 m + 0.022 \log^4 m$ (‡) | 1.76 | V | 22 |

which contradicts Equation 45h for v^{\square} at $x = 1$ since the sum of the volume changes across the whole cell is non-zero. It follows that the model can have no exact solution in a one-dimensional setting. This can be resolved by considering a multi-dimensional problem with a free electrolyte surface; this solution is beyond the present scope. For the present purposes, we take the limit in which β_n and β_p are zero (note, from Table I, that β_n and β_p are small).

ORCID

Valentin Sulzer  <https://orcid.org/0000-0002-8687-327X>
 S. Jon Chapman  <https://orcid.org/0000-0003-3347-6024>
 Colin P. Please  <https://orcid.org/0000-0001-8917-8574>
 David A. Howey  <https://orcid.org/0000-0002-0620-3955>
 Charles W. Monroe  <https://orcid.org/0000-0002-9894-5023>

References

- G. Richardson, G. Denuault, and C. P. Please, Multiscale modeling and analysis of lithium-ion battery charge and discharge, *Journal of Engineering Mathematics*, **72**(1), 41 (2012).
- M. Schmuck and M. Z. Bazant, Homogenization of the Poisson–Nernst–Planck equations for ion transport in charged porous media, *SIAM Journal on Applied Mathematics*, **75**(3), 1369 (2015).
- J. A. Trainor III, Flow-through porous electrodes, *Lawrence Berkeley National Laboratory*, 2011.
- J. Liu and C. W. Monroe, Solute-volume effects in electrolyte transport, *Electrochimica Acta*, **135**, 447 (2014).
- V. Sulzer, S. J. Chapman, C. P. Please, D. A. Howey, and C. W. Monroe, Faster Lead-Acid Battery Simulations from Porous-Electrode Theory: Part II. Asymptotic Analysis, *Journal of The Electrochemical Society*, **166**(12), 2372 (2019).
- B. Culpin, Thermal runaway in valve-regulated lead-acid cells and the effect of separator structure, *Journal of Power Sources*, **133**(1), 79 (2004).
- F. J. Vaccaro and R. E. Landwehrle, Experiments on thermal run-a-way and its management for electrolyte immobilized lead-acid batteries. In *Telecommunications Energy Conference, 1991. INTELEC'91., 13th International*, pages 20–25. IEEE, 1991.
- W. B. Gu, G. Q. Wang, and C. Y. Wang, Modeling the overcharge process of vrla batteries, *Journal of Power Sources*, **108**(1), 174 (2002).
- V. Srinivasan and C. Y. Wang, Analysis of electrochemical and thermal behavior of li-ion cells, *Journal of The Electrochemical Society*, **150**(1), A98 (2003).
- D. M. Bernardi and M. K. Carpenter, A mathematical model of the oxygen-recombination lead-acid cell, *Journal of The Electrochemical Society*, **142**(8), 2631 (1995).
- M. Cugnet and B. Y. Liaw, Effect of discharge rate on charging a lead-acid battery simulated by mathematical model, *Journal of Power Sources*, **196**(7), 3414 (2011).
- J. Newman and W. Tiedemann, Simulation of recombinant lead-acid batteries, *Journal of The Electrochemical Society*, **144**(9), 3081 (1997).
- D. M. Bernardi, H. Gu, and A. Y. Schoene, Two-dimensional mathematical model of a lead-acid cell, *Journal of The Electrochemical Society*, **140**(8), 2250 (1993).
- H. Gu, T. V. Nguyen, and R. E. White, A mathematical model of a lead-acid cell discharge, rest, and charge, *Journal of The Electrochemical Society*, **134**(12), 2953 (1987).
- W. B. Gu, C. Y. Wang, and B. Y. Liaw, Numerical modeling of coupled electrochemical and transport processes in lead-acid batteries, *Journal of The Electrochemical Society*, **144**(6), 2053 (1997).
- P. Goyal and C. W. Monroe, New foundations of Newman's theory for solid electrolytes: Thermodynamics and transient balances, *Journal of The Electrochemical Society*, **164**(11), E3647 (2017).
- T. W. Chapman and J. Newman, Compilation of selected thermodynamic and transport properties of binary electrolytes in aqueous solution. *Technical report*, California Univ., Berkeley. Lawrence Radiation Lab., 1968.
- J. Liu, S. K. Rahimian, and C. W. Monroe, Capacity-limiting mechanisms in li/o2 batteries, *Physical Chemistry Chemical Physics*, 2016.
- C. W. Monroe and Charles Delacourt, Continuum transport laws for locally non-neutral concentrated electrolytes, *Electrochimica Acta*, **114**, 649 (2013).
- J. Newman and T. W. Chapman, Restricted diffusion in binary solutions, *AIChE Journal*, **19**(2), 343 (1973).
- A. M. Bizeray, D. A. Howey, and C. W. Monroe, Resolving a discrepancy in diffusion potentials, with a case study for li-ion batteries, *Journal of The Electrochemical Society*, **163**(8), E223 (2016).
- H. Bode, *Lead-acid batteries*. John Wiley & Sons, Inc., New York, NY, 1977.
- V. Srinivasan, G. Q. Wang, and C. Y. Wang, Mathematical modeling of current-interrupt and pulse operation of valve-regulated lead acid cells, *Journal of The Electrochemical Society*, **150**(3), A316 (2003).
- V. Sulzer, Faster Lead-Acid Models. Software on Zenodo, 2019.
- E. Jones, T. Oliphant, and P. Peterson et al. SciPy: Open source scientific tools for Python, 2001–. [Online; accessed 23/03/2018].
- C. Cartis and L. Roberts, A derivative-free gauss-newton method, *arXiv preprint arXiv:1710.11005*, 2017.
- A. F. Bower, P. R. Guduru, and V. A. Sethuraman, A finite strain model of stress, diffusion, plastic flow, and electrochemical reactions in a lithium-ion half-cell, *Journal of the Mechanics and Physics of Solids*, **59**(4), 804 (2011).
- M. J. Chon, V. A. Sethuraman, Anthony McCormick, V. Srinivasan, and P. R. Guduru, Real-time measurement of stress and damage evolution during initial lithiation of crystalline silicon, *Physical Review Letters*, **107**(4), 045503 (2011).
- V. A. Sethuraman, M. J. Chon, Maxwell Shimshak, Nathan Van Winkle, and P. R. Guduru, In situ measurement of biaxial modulus of si anode for li-ion batteries, *arXiv preprint arXiv:1108.0567*, 2011.
- V. A. Sethuraman, M. J. Chon, Maxwell Shimshak, V. Srinivasan, and P. R. Guduru, In situ measurements of stress evolution in silicon thin films during electrochemical lithiation and delithiation, *Journal of Power Sources*, **195**(15), 5062 (2010).
- V. A. Sethuraman, V. Srinivasan, A. F. Bower, and P. R. Guduru, In situ measurements of stress-potential coupling in lithiated silicon, *Journal of The Electrochemical Society*, **157**(11), A1253 (2010).
- V. A. Sethuraman, Kristin Kowolik, and V. Srinivasan, Increased cycling efficiency and rate capability of copper-coated silicon anodes in lithium-ion batteries, *Journal of Power Sources*, **196**(1), 393 (2011).
- P. Goyal and C. W. Monroe, Exploring the impedance signatures of electrochemical/mechanical transport coupling in concentrated liquid electrolytes. In *Meeting Abstracts*, number 22, pages 1137–1137. *The Electrochemical Society*, 2017.
- R. S. Treptow, The lead-acid battery: Its voltage in theory and in practice, *Journal of Chemical Education*, **79**(3), 334 (2002).
- V. Boovaragavan, R. N. Methakar, V. Ramadesigan, and V. R. Subramanian, A mathematical model of the lead-acid battery to address the effect of corrosion, *Journal of The Electrochemical Society*, **156**(11), A854 (2009).
- J. Cao, Private communication (email). 2016.
- D. R. Lide and H. P. R. Frederikse, *CRC handbook of chemistry and physics: a ready-reference book of chemical and physical data*, volume 83. Boca Raton: CRC Press LLC, 1992.
- W. H. Tiedemann and J. Newman, Battery design and optimization, *Journal of Electrochemical Society, Softbound Proceeding Series*, Princeton, New York, **79**(1), 23 (1979).
- K. S. Pitzer, R. N. Roy, and L. F. Silvester, Thermodynamics of electrolytes. 7. sulfuric acid, *Journal of the American Chemical Society*, **99**(15), 4930 (1977).
- J. Newman and K. E. Thomas-Alyea, *Electrochemical Systems*, 3rd Ed., John Wiley & Sons, 2004.